ACS APPLIED MATERIALS & INTERFACES

RESEARCH ARTICLE

www.acsami.org

Adhesive-Free Transfer of Gold Patterns to PDMS-Based Nanocomposite Dielectric for Printed High-Performance Organic Thin-Film Transistors

Jingsheng Shi, Mary B. Chan-Park, and Chang Ming Li*

Center for Advanced Bionanosystems School of Chemical and Biomedical Engineering, Nanyang Technological University, 70 Nanyang Drive, 637457 Singapore

Supporting Information

ABSTRACT: Low-cost, adhesive-free direct transfer of gold patterns onto PDMS-based nanocomposite dielectric layer was investigated to significantly improve contact resistance at electrode−semiconductor interface in organic thin-film transistors (OTFTs). In particular, the nanocomposite film made from PDMS and solution-processable titanium dioxide nanoparticles was applied as dielectric layer in OTFTs, while transfer of gold patterns with a resolution lower than 3 μm is realized without use of any adhesive but through increased adhesion between gold and nanocomposite film of higher thickness and dielectric constant formed by in situ PDMS cross-linking process. Dielectric constant of the nanocomposite shows a dependence on the ratio of titanium dioxide nanoparticles to PDMS and the dielectric thickness was optimized for the best transfer efficiency. The organic transistors fabricated by this process demonstrate a high mobility of 0.038 $cm^2/(V\ s)$ and on/off ratio of 1×10^4 to 1×10^5. The electrode-semiconductor interface is evaluated by transmission line model to have width-normalized contact resistance of ~100 kΩ cm while the inert property of dielectric-semiconductor interface gives low hysteresis (ΔV_{th} = 1.2 V) and low threshold voltage (V_{th} = −1.3 V) in the devices. This process can be readily adapted into a low-cost mass manufacturing process for printed organic electronics.

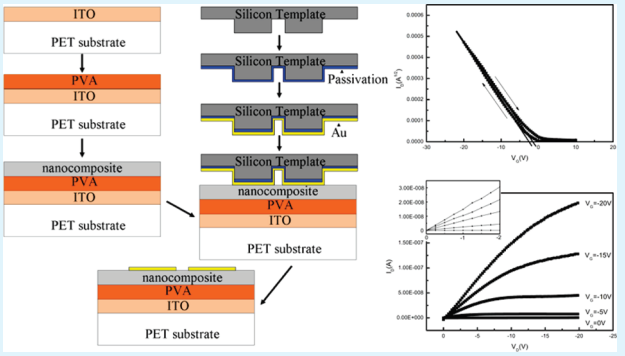

KEYWORDS: electrode-semiconductor interface, organic thin-film transistor, semiconductor-dielectric interface, transfer printing, nanocomposite, PDMS, titanium oxide nanoparticle

INTRODUCTION

Research and development of organic electronics such as organic thin-film transistors (OTFTs), organic light-emitting diodes (OLEDs) and organic photovoltaic devices as low-cost alternatives for the conventional semiconductor devices have rapidly increased in the past few years.[1−4] Unlike the traditional inorganic semiconductor process, the low-temperature solution-based processes used for printed organic electronics can deposit various organic semiconductors on a broad range of substrate materials such as plastics to fabricate low-cost electronics under ambient conditions.[5,6] The continuous efforts to reduce the cost of organic electronics require a suitable printing process that is independent of expensive photolithography. Inkjet printing,[7,8] gravure printing,[9] and transfer printing[10,11] have been reported to meet the needs of the emerging low-cost organic electronics.

In printing technology, the transfer of Au film from the surface of a template onto a substrate for a patterned gold structure has been studied. Much of the efforts have been devoted to print patterned Au films onto rigid substrates by using elastomeric stamps, while the substrates are derivatized with self-assembled monolayers (SAM) of molecules with thiol function group as an adhesive for the Au film.[12−14] A few studies have reported the use of rigid stamps such as patterned Si wafers to print patterned Au films onto a cross-linked solid PDMS modified with thiolated SAM as a molecular adhesive or Ti/Cr as a metallic adhesive for Au film transfer,[15,16] where the PDMS simply serves as an elastomeric substrate. However, the adhesion between the Au film and substrate such as Ti can adversely affect charge injection in the electrode-semiconductor interface to cause a significantly elevated interfacial contact resistance and deteriorate the device performance.[17] A direct transfer process of Au film onto PDMS surface without any adhesive interlayer is advantageous for improved device performance since PDMS as a dielectric material, instead of merely substrate material, has its unique advantages. It allows fabricating extremely flat films, provided that the prepolymer is cast and spun over a very flat substrate. More importantly, it has a hydroxyl-free and inert surface after curing, making it an excellent candidate to fabricate organic transistors

Received: January 17, 2011
Accepted: May 2, 2011
Published: May 02, 2011

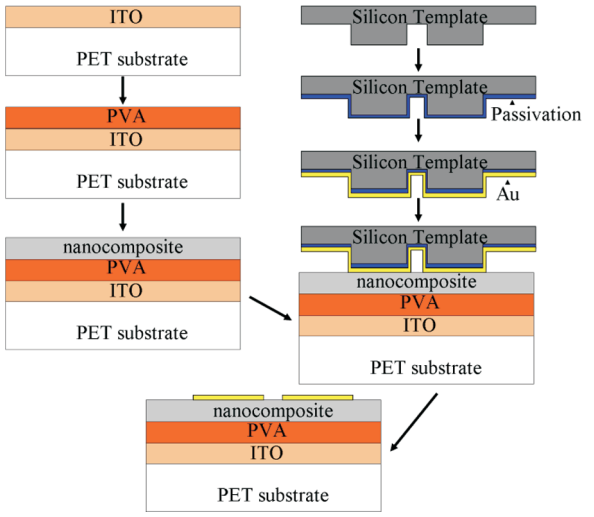

Figure 1. Schematic illustration of the direct transfer printing process on PDMS-based nanocomposite.

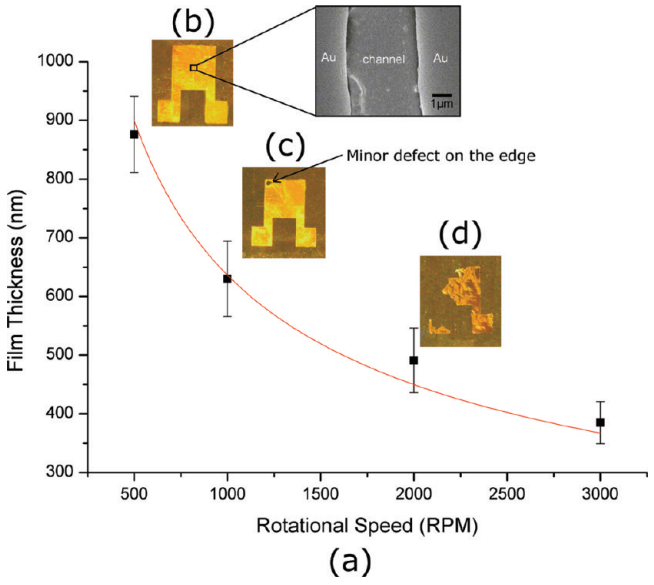

Figure 2. (a) Thickness of spin-coated nanocomposite film versus different spin speed; (b–d) gold patterns transferred onto the nanocomposite film with the thickness represented by the corresponding data points; the inset shows an SEM image of the channel between Au electrodes with a resolution of 3 μm.

with possible n-type conduction[18−20] and low hysteresis.[21] However, PDMS is a low-K dielectric material, and needs to be fabricated into a very thin film for effective gate modulation and thus elimination of short-channel effect (SCE) becomes very difficult, especially in devices with a short channel length.[22,23]

In this work, we demonstrate a novel direct transfer process to fabricate Au pattern without use of any adhesive but by increasing adhesion between Au and nanocomposite surfaces through an in situ PDMS cross-linking process. In the process, the liquid prepolymer surrounding titanium dioxide nanoparticles cross-links and produce the solid nanocomposite film with higher adhesion to Au surface to facilitate the transfer process. Titanium dioxide nanoparticles of about 4 − 8 nm in size with dielectric constant of about 5.3 has been synthesized with a solution process,[24] which is highly compatible with PDMS by choosing a common solvent for both materials to disperse the nanoparticles uniformly in PDMS and further fabricate the PDMS-based nanocomposite dielectric layer with a higher dielectric constant than plain PDMS. The transferred Au film, with a resolution down to 3 μm (shown in the inset of Figure 2) limited by the resolution of master template, can easily survive Scotch Tape test and the bottom-gated organic transistors were fabricated by this process using poly(3,3‴-didodecylquaterthiophene) (PQT-12) as the active material to demonstrate the advantages of the process and its great potential in organic electronics.

EXPERIMENTAL SECTION

Materials. 1H,1H,2H,2H-perfluoro-octyl triethoxysilane, indium tin oxide (ITO) coated Poly(ethylene terephthalate) (PET) films, Poly(vinyl alcohol) (PVA), hexane, toluene, chloroform, gold and aluminum sputtering targets were purchased from Sigma-Aldrich (Singapore), silicon wafers were purchased from Bonda Technology (Singapore), PDMS Sylgard 184 was purchased from Dow Corning (Midland, MI, USA). Preparation of titanium dioxide nanoparticles solution was described in reference.[24] PQT-12 was prepared with the quaterthiophene monomer (3,3‴-Didodecylquaterthiophene) by $FeCl_3$-mediated oxidative coupling polymerization.[25] In particular, after the quaterthiophene monomer was added in $FeCl_3$ suspension with an appropriate solvent at room temperature (typically 6.2 g quaterthiophene monomer to 20.4 g $FeCl_3$ suspension in 250 mL chloroform), the mixture was stirred for 20 min, and then water was added into the reaction vessel to terminate the polymerization. The polymer was then washed with water, precipitated with acidic ethanol and filtered. The product was further extracted and purified with heptane and chlorobenzene to give electrically pure 0.3 wt % PQT-12 solution in chlorobenzene for OTFT fabrication. All chemicals used in PQT-12 synthesis process were also purchased from Sigma-Aldrich.

Instruments. Deep reactive ion etcher (Surface Technology Systems, Newport, U.K.) was used in fabrication of silicon template. Nanocomposite thin-films were prepared using G3P-8 spin-coater (Specialty Coating Systems, Indianapolis, IN). Deposition of gold and aluminum thin-films was performed on explorer series sputtering system (Denton Vacuum, Moorestown, NJ, USA). Agilent 4284A precision LCR meter (Agilent, Santa Clara, CA, USA) was used to measure the capacitance of ITO-nanocomposite-Al capacitors. JSM-6700F field emission scanning electron microscopy (FE-SEM) (JEOL Ltd., Tokyo, Japan) was used to characterize the surface and cross-section of nanocomposite films. Atomic force microscopy (AFM) measurements of nanocomposite film thickness were performed on a Dimension 3100/Nanoscope IIIa (Digital Instruments, Santa Barbara, CA, USA) in tapping mode. Annealing of organic semiconductor film was conducted in EYELA VOS-201SD vacuum drying oven (Tokyo Rikakikai, Tokyo, Japan). SMZ1500 optical microscope (Nikon Instruments Inc., Melville, NY, USA) was used to characterize the transferred gold patterns. Characterization of organic thin-film transistors was performed on Summit series probe station (Cascade Microtech, Beaverton, OR, USA) and E5270B semiconductor analyzer (Agilent, Santa Clara, CA, USA). All the baking processes in air were conducted in heating oven (Memmert GmbH + Co.KG, Schwabach, Germany).

Preparation of PDMS−Titanium Dioxide Nanocomposite. Sylgard 184 PDMS prepolymer and curing agent with weight ratio of 1:1 were dissolved in toluene to form a 20 wt % solution; 0.5 g of PDMS solution was mixed with 0.5 g of 3.5 wt % organic-capped titanium dioxide nanoparticles solution in chloroform. The amount of nanoparticles solution was controlled to obtain different ratio of titanium dioxide nanoparticles to PDMS in nanocomposite solution. The added curing agent was excessive since it was found that a longer curing time than the

Table 1. Transfer Efficiency with Different Nanocomposite Film Thicknesses

nanocomposite film thickness (nm)	total number of samples	intact patterns transferred (Figure 2b)	patterns with minor defects (Figure 2c)
880 ± 60	15	14	1
630 ± 60	15	5	10
490 ± 45	15	2	3

recommended was often required. The prepared nanocomposite solution was immediately spin-coated on ITO-coated PET film to form nanocomposite films with different thicknesses by controlling spin speed. Before spin coating process, ITO-coated PET films were cleaned by sonication in decon 90 cleaning agent for 10 min, rinsed with DI water to remove the remnant detergent and blown dry by air. The nanocomposite films were then baked at 150 °C for 3−5 h to fully cross-link the nanocomposite into a solid film.

Characterization of Nanocomposite Film. The surface and cross-section of the nanocomposite films were characterized by FE-SEM. The nanocomposite film samples for cross-sectional view were prepared in liquid nitrogen. The thicknesses of the nanocomposite films were measured by AFM. To measure the thickness, a nanocomposite film was partially removed from ITO coated PET film to create a step in the nanocomposite film and AFM tip scanned across the step to measure the height of it, which was taken as the thickness of the nanocomposite film. 100 nm aluminum was deposited on the nanocomposite film using sputtering system to fabricate ITO-nanocomposite-Al capacitors. For each nanoparticle to PDMS ratio, six capacitors were fabricated and the capacitances of these capacitors were measured using probe station and Agilent LCR meter. The average value of the measured capacitances was used to calculate the dielectric constant of the nanocomposite film.

Fabrication of Organic Thin-Film Transistors. A schematic illustration for the fabrication procedure of an organic transistor device in bottom-gated configuration is shown in Figure 1. To fabricate the organic transistor, we first fabricated silicon template via standard procedures of photolithography and deep reactive ion etching (DRIE). The etching depth was 100−150 μm. One millimolar 1H,1H,2H,2H-perfluoro-octyl triethoxysilane in hexane solution was used to form a self-assembled monolayer (SAM) as a passivation layer on the silicon template. 100 nm gold was sputtered onto the passivated silicon template. 5% PVA solution in DI water was spin-coated on ITO coated PET film to form a PVA dielectric layer of about 200 nm for reduced parasitic gate leakage current. ITO served as the transistor gate electrode. The prepared nanocomposite solution was then spin-coated on the PVA dielectric layer to form an 880 ± 60 nm thick nanocomposite layer, followed by baking at 150 °C for 2 min to remove the remnant solvent. Longer baking time should be avoided to prevent excessive curing of PDMS in the nanocomposite before contact with the silicon template. To calculate mobility of device, the unit area capacitance of the dielectric layer stack including PVA and nanocomposite layer (2.68 nF/cm^2) was measured separately by fabricating ITO-insulator-Al capacitors. The coated substrate was carefully brought into contact with the gold-coated silicon template. Gentle pressure was applied to ensure sufficient contact between the nanocomposite film and gold. The whole assembly was then baked at 150 °C for 3−5 h to fully cross-link the nanocomposite into a solid film. The cross-linking process of the nanocomposite could increase the adhesion between gold and nanocomposite after nanocomposite turning from liquid into solid film. This explains why the gold film can be transferred onto the nanocomposite film without need of an additional adhesive. After demolding, the gold film was transferred onto the nanocomposite film to form the transistor source and drain electrodes. PQT-12 solution in chlorobenzene with a concentration of 0.3 wt %[25] was drop-casted and annealed at 150 °C for 45 min in a vacuum oven as the active layer to complete OTFT fabrication. Apparently, this approach can provide a low-cost mass printing manufacturing process for printed organic electronics.

Characterization of Organic Thin-Film Transistors. The OTFTs were characterized in ambient air using an Agilent E5270B semiconductor analyzer and probe station. The output characteristics of the OTFTs was obtained by sweeping the drain voltage from 0 V to −20 V and stepping the gate voltage from 0 V to −20 V at an interval of 5 V. The transfer characteristics of the OTFTs was obtained by keeping the drain voltage constant at −20 V and sweeping the gate voltage from 10 V to −20 V as off-to-on direction and from −20 to 10 V as on-to-off direction. Study of contact resistance by transmission line model was conducted by measuring resistances between the source and drain electrodes for different channel lengths with different gate voltages applied using the same equipments.

RESULTS AND DISCUSSION

Dependence of Transfer Efficiency on Nanocomposite (PDMS) Film Thickness. On the basis of the experimental results of spin coating different polymer solutions with different solvents on silicon wafer and measuring film thicknesses with ellipsometry, an empirical formula on the dependence was concluded by C. J. Lawrence for polymer solutions correlating the thin-film thickness with spin speeds as[26]

$$h_f \propto \Omega^b \quad (1)$$

where h_f is the resulted polymer film thickness, Ω is the spin speed with unit of revolutions per minute (RPM), and b is an empirical constant of −1/2. To study whether the spin-coated film thickness can be predicted using this empirical relationship, we measured the thicknesses of nanocomposite films fabricated with different spin speeds by AFM. Figure 2a shows the thickness against spin speed and the polynomial fit by setting $b = -1/2$, illustrating that the film thickness can be predicted closely by the empirical formula at lower spin speeds, whereas the measured thickness is higher than that predicted by 20−30 nm at higher spin speeds.

By transfer-printing gold patterns onto the nanocomposite film of different thicknesses, a significant dependence of gold transfer efficiency on the nanocomposite film thickness was observed. Figure 2b−d demonstrate that gold pattern transferred onto the 880 ± 60 nm thick nanocomposite film is intact while gold pattern transferred on the 630 ± 60 nm thick nanocomposite film is still almost intact except a minor defect at the edge of the pattern. However, the gold transferred onto the 490 ± 45 nm thick nanocomposite film with a broken pattern is taken as failed transfer. Table 1 shows the statistical data of the transfer efficiency in correlation with nanocomposite film with different thickness.

Three batches of gold patterns with 15 gold patterns in each batch were fabricated under the same conditions except the thickness of the nanocomposite film. The intact patterns are the patterns without defect as shown in Figure 2b, whereas patterns with minor defect are the gold patterns that have minor defect on the edge of the pattern but the transistor channel between source and drain electrodes is successfully created (shown in Figure 2c). Gold patterns transferred like the one in Figure 2d are not taken into account as successfully transferred patterns.

The surfaces of nanocomposite thin films were characterized by FE-SEM as shown in Figure 3. In the SEM images, titanium dioxide nanoparticle aggregates can be observed in the nanocomposite

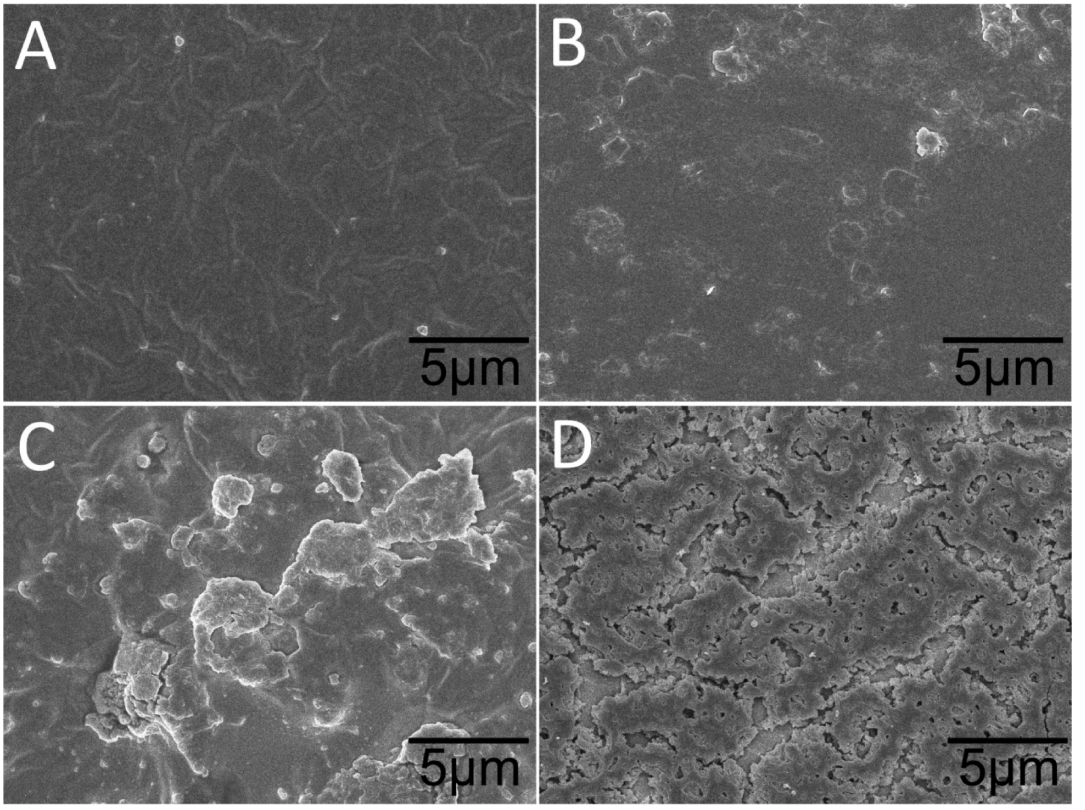

Figure 3. (A−C) FE-SEM images of film surfaces with 880, 630, and 490 nm thicknesses, respectively; (D) FE-SEM image of pure titanium dioxide nanoparticle film surface (cross-sectional view of the films are provided in the Supporting Information).

films with different thicknesses studied. In the 880 nm thick nanocomposite film, the surface mainly comprises PDMS with a typical ripplelike polymer surface and a few aggregates of titanium dioxide nanoparticles with diameter of about 200 nm. In the 630 nm thick nanocomposite film, more titanium dioxide nanoparticle aggregates sized about 1 μm emerge on the surface and the ripplelike polymer surface becomes less apparent. In the nanocomposite film with thickness of 490 nm, the surface is mainly composed of titanium dioxide nanoparticle aggregates sized about 5 μm. In fact, the composition and thickness of the nanocomposite film are dependent on the spin speed. More nanoparticles with much lower solubility than PDMS can precipitate to form larger aggregates due to faster solvent evaporation when using higher spin speed to make a thinner film. Good contact between gold pattern and nanocomposite film is crucial for successful transfer. The silicon template used in the process is a hard template, which lacks flexibility and has better contact with only thicker soft films.[27] Furthermore, larger nanoparticle aggregates in a thinner film can impede good contact between the two surfaces, resulting lower transfer efficiency. This explains the dependence of transfer efficiency on nanocomposite film thickness. Thus, a certain thickness of the nanocomposite film as the dielectric layer is necessary to possess good contact and high adhesion for the pattern transfer. This can also explain that a pure PDMS cannot be directly used for an adhesive-free pattern transfer process since thick PDMS film cannot be used as transistor dielectric layer because of its low dielectric constant as discussed in more detail below.

Dielectric Constant of Nanocomposite. Pure PDMS without titanium dioxide nanoparticles as the dielectric material has been investigated in this work. Due to the low dielectric constant of PDMS (2.3−2.8),[28] a very thin PDMS film (500−600 nm) must be used to effectively avoid SCE in transistor devices with a channel length around 3 μm in terms of our experimental results. However, the yield of this process drops to an unacceptable value that cannot be used in a practical manufacturing process since all transfer processes tried with pure PDMS film of about 500 nm thickness failed by results similar to Figure 2d. One approach to

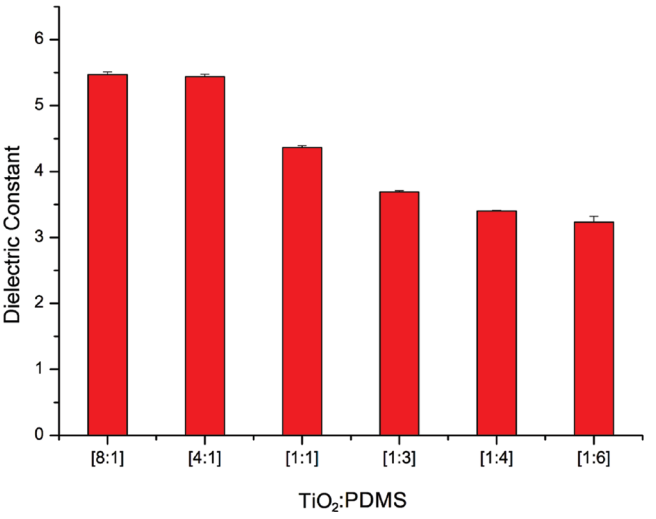

Figure 4. Dielectric constant of the nanocomposite material with different weight ratio of titanium dioxide nanoparticles to PDMS.

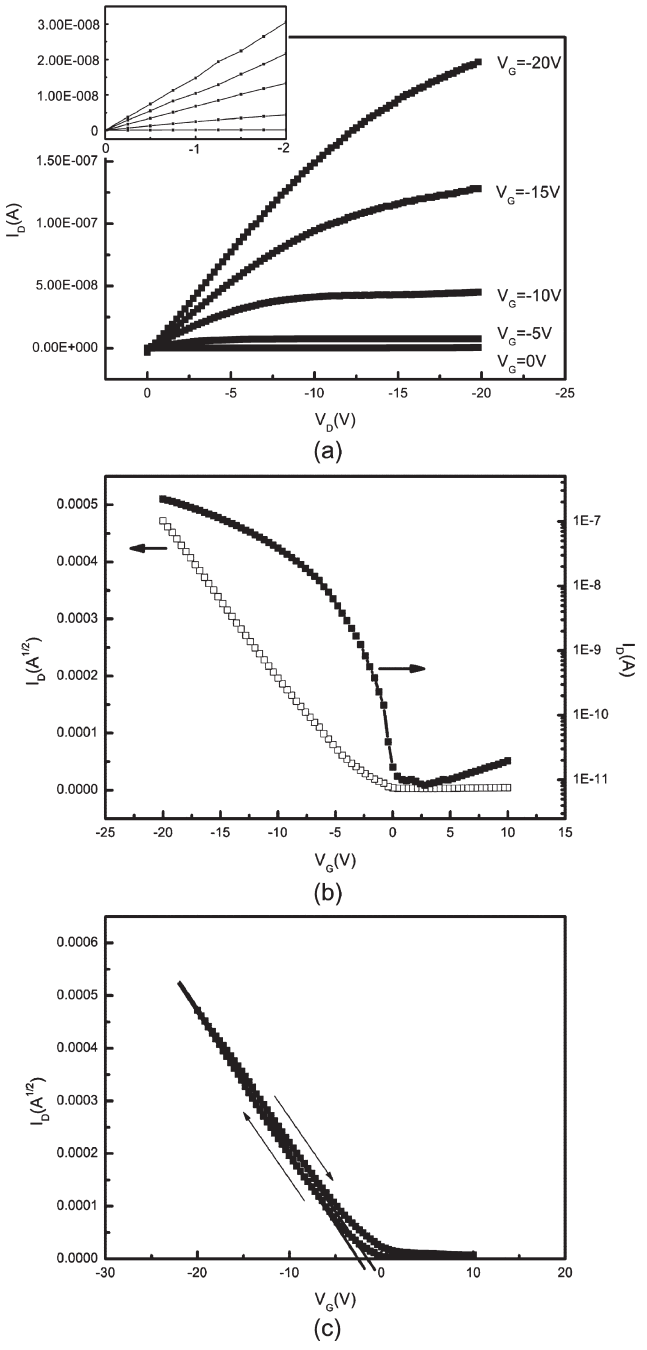

Figure 5. Representative performance of organic transistors fabricated with the reported process (a) source-drain current versus source-drain voltage with different gate voltage applied, the inset shows source-drain current versus source-drain voltage at the linear region, indicating an ideal ohmic contact between the direct transferred gold patterns and the active material; (b) transfer characteristics of the devices; (c) plot of square root of source-drain current against gate voltage, source-drain current is measured when gate voltage is swept in both off-to-on and on-to-off directions. Linear fits of both directions are shown in order to find the corresponding threshold voltage.

solve this dilemma is to increase the dielectric constant of the dielectric material. Solution-processable organic-capped titanium dioxide nanoparticle solution[24] was mixed with PDMS solution with proper concentration to produce nanocomposite material with a higher dielectric constant. Figure 4 shows the

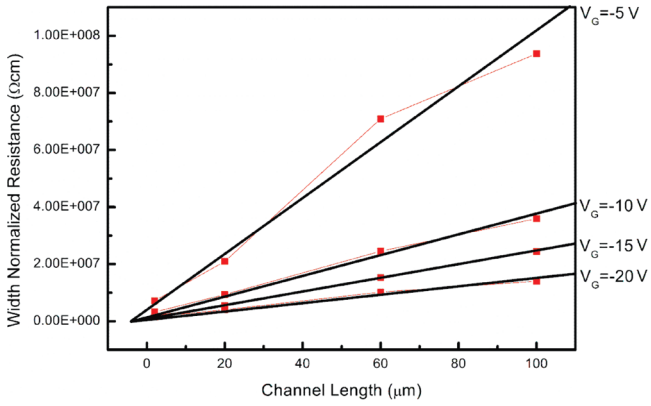

Figure 6. Dependence of width-normalized total ON resistance on channel length of the devices. Drain voltage is −2 V and gate voltages are −20, −15, −10, and −5 V.

dielectric constant of the nanocomposite against the weight ratio of titanium dioxide nanoparticles to PDMS. The dielectric constant of the nanocomposite increases with increasing ratio of titanium dioxide nanoparticle to PDMS until achieving a plateau to have the maximum dielectric constant (∼5.3), which is almost the same as titanium dioxide nanoparticles. Because a thinner film would be fabricated with higher nanoparticle to PDMS ratio under the same spin coating parameters, a weight ratio of 1:6 (titanium dioxide nanoparticle: PDMS) was chosen in order to satisfy the thickness requirement in this process.

Performance of Bottom-Gated OTFTs Using PDMS-Based Nanocomposite Dielectric. Figure 5 shows the output and transfer characteristics of organic transistors fabricated with the direct transfer process. The transistor devices were characterized as described in the Experimental Section. From panels a and b in Figure 5, a mobility of 0.038 $cm^2/(V\,s)$ in saturation regime and on/off ratio of 1×10^4 to 1×10^5 are extracted using

$$\mu = \left(\frac{\partial\sqrt{I_D}}{\partial V_G}\right)^2 \frac{2L}{W}\frac{1}{C_i} \qquad (2)$$

where I_D is the drain current, C_i is the capacitance per unit area of the gate dielectric film, and V_G is the gate voltage. V_{th} of the device was estimated to be −1.3 V from the intersection between $I_D = 0$ and linear fit of $I_D^{1/2} - V_G$ curve at the saturation regime.

Figure 5c shows the hysteresis characteristic of the transistor device by measuring root square of drain current while the gate voltage is swept in both off-to-on and on-to-off directions. Two lines are fit to the bidirectional curve and threshold voltages are obtained by extrapolating the fitting lines to $I_D^{1/2} = 0$. The obtained threshold voltage when gate voltage is swept from off-state (V_G = 10 V) to on-state (V_G = −20 V) is $V_{th(off\text{-}to\text{-}on)}$ = −2.5 V, whereas the corresponding threshold voltage when the gate voltage is swept from on-state to off-state is $V_{th(on\text{-}to\text{-}off)}$ = −1.3 V, which gives a very small ΔV_{th} = 1.2 V. This value, in particular considering that all measurements were conducted in ambient air, is much smaller than ΔV_{th} on silicon dioxide,[29] HMDS treated silicon dioxide,[30] poly (4-vinylphenol)[31] and other different hydroxyl-containing polymer dielectrics[32] reported in the literature. The small swing of threshold voltage demonstrating the low hysteresis behavior in the device can be attributed principally to the hydroxyl-free nature of dielectric-semiconductor interface suggested by Bao et al.[21]

To demonstrate the low contact resistance between the active material and direct transfer-printed source and drain electrodes

without adhesives, the response at small source-drain voltages is shown in the inset of Figure 5a. The good linear response of transistor at the linear region suggests ideal ohmic contacts with low contact effects between the transferred electrodes and active organic semiconductor in the transistor channel. To further study the electrode-semiconductor interface, transmission line model[33] relating the channel length and width-normalized total resistance in the device was used to estimate the contact resistance at source and drain contacts

$$R_{\text{total}} = \left.\frac{\partial V_D}{\partial I_D}\right|_{V_D \to 0}^{V_G} = R_{\text{ch}} + R_C = \frac{L}{W\mu C_i(V_G - V_T)} + R_C \quad (3)$$

and width-normalized resistance:

$$R_{\text{total}}W = \frac{L}{\mu C_i(V_G - V_T)} + R_C W \quad (4)$$

Figure 6 shows width-normalized device resistance versus channel length of transistors and the linear fit of the data points. By extrapolating the linear fit to $L = 0$, the contact resistance in the transistor devices is estimated to be on the order of ~100 kΩ cm. This value is less than or comparable to the contact resistance at gold-semiconductors interface optimized by reduced adhesive thickness, hole injection layer or sulfuric acid treatment on electrodes.[34−37]

CONCLUSION

In summary, a low-cost adhesive-free direct transfer printing process onto PDMS-based nanocomposite dielectric material with a resolution down to 3 μm was developed and successfully applied in fabrication of organic thin-film transistors. Dielectric constant of the nanocomposite was observed to vary with the ratio of titanium dioxide nanoparticle to PDMS. With optimized nanocomposite thickness, the transfer efficiency of gold patterns can achieve a very high level while avoiding short-channel effect in the fabricated organic transistors. The organic transistors fabricated by this process showed a high mobility of 0.038 $cm^2/(V\ s)$ and on/off ratio of 1×10^4 to 1×10^5. Due to the inert nature of the dielectric-semiconductor interface, transistor devices also demonstrate low hysteresis ($\Delta V_{th} = 1.2$ V) and low threshold voltage (−1.3 V). Width-normalized contact resistance between the transfer-printed gold patterns and active material in organic transistors is on the order of ~100 kΩ cm, which is due to the absence of SAM or metallic adhesive at the electrode-semiconductor interface. This technique can be readily adapted into low-cost mass manufacturing process for printed organic electronics.

ASSOCIATED CONTENT

Supporting Information. SEM images of cross-sections of nanocomposite films. This material is available free of charge via the Internet at http://pubs.acs.org/.

AUTHOR INFORMATION

Corresponding Author

*Corresponding author. E-mail: ecmli@ntu.edu.sg.

ACKNOWLEDGMENT

This work was financially supported by Singapore National Research Foundation Grant under NRF-CRP2-2007-02.

REFERENCES

(1) Brown, A. R.; Pomp, A.; Hart, C. M.; de Leeuw, D. M. *Science* **1995**, *270*, 972–974.
(2) Burroughes, J. H.; Bradley, D. D. C.; Brown, A. R.; Marks, R. N.; Mackay, K.; Friend, R. H.; Burns, P. L.; Holmes, A. B. *Nature* **1990**, *347*, 539–541.
(3) Yu, G.; Gao, J.; Hummelen, J. C.; Wudl, F.; Heeger, A. J. *Science* **1995**, *270*, 1789–1791.
(4) Acton, B. O.; Ting, G. G.; Shamberger, P. J.; Ohuchi, F. S.; Ma, H.; Jen, A. K. Y. *ACS Appl. Mater. Interfaces* **2010**, *2*, 511–520.
(5) Kagan, C. R.; Breen, T. L.; Kosbar, L. L. *Appl. Phys. Lett.* **2001**, *79*, 3536–3538.
(6) Gan, Y.; Cai, Q. J.; Li, C. M.; Yang, H. B.; Lu, Z. S.; Gong, C.; Chan-Park, M. B. *ACS Appl. Mater. Interfaces* **2009**, *1*, 2230–2236.
(7) Sirringhaus, H.; Kawase, T.; Friend, R. H.; Shimoda, T.; Inbasekaran, M.; Wu, W.; Woo, E. P. *Science* **2000**, *290*, 2123–2126.
(8) Doggart, J.; Wu, Y.; Liu, P.; Zhu, S. *ACS Appl. Mater. Interfaces* **2010**, *2*, 2189–2192.
(9) Tobjörk, D.; Kaihovirta, N. J.; Mäkelä, T.; Pettersson, F. S.; Österbacka, R. *Org. Electron.* **2008**, *9*, 931–935.
(10) Hines, D. R.; Ballarotto, V. W.; Williams, E. D.; Shao, Y.; Solin, S. A. *J. Appl. Phys.* **2007**, *101*, 024503.
(11) Zhang, J.; Li, C. M.; Chan-Park, M. B.; Zhou, Q.; Gan, Y.; Qin, F.; Ong, B.; Chen, T. *Appl. Phys. Lett.* **2007**, *90*, 243502.
(12) Menard, E.; Bilhaut, L.; Zaumseil, J.; Rogers, J. A. *Langmuir* **2004**, *20*, 6871–6878.
(13) Meitl, M. A.; Zhu, Z.-T.; Kumar, V.; Lee, K. J.; Feng, X.; Huang, Y. Y.; Adesida, I.; Nuzzo, R. G.; Rogers, J. A. *Nat. Mater.* **2006**, *5*, 33–38.
(14) Loo, Y.-L.; Hsu, J. W. P.; Willett, R. L.; Baldwin, K. W.; West, K. W.; Rogers, J. A. *46th International Conference on Electron, Ion, and Photon Beam Technology and Nanofabrication*; Anaheim, CA, May 28−31, 2002; American Vacuum Society: New York, 2002; pp 2853−2856.
(15) Loo, Y. L.; Willett, R. L.; Baldwin, K. W.; Rogers, J. A. *J. Am. Chem. Soc.* **2002**, *124*, 7654–7655.
(16) Loo, Y.-L.; Willett, R. L.; Baldwin, K. W.; Rogers, J. A. *Appl. Phys. Lett.* **2002**, *81*, 562–564.
(17) Yoneya, N.; Noda, M.; Hirai, N.; Nomoto, K.; Wada, M.; Kasahara, J. *Appl. Phys. Lett.* **2004**, *85*, 4663–4665.
(18) Chua, L.-L.; Zaumseil, J.; Chang, J.-F.; Ou, E. C. W.; Ho, P. K. H.; Sirringhaus, H.; Friend, R. H. *Nature* **2005**, *434*, 194–199.
(19) Orgiu, E.; Manunza, I.; Sanna, M.; Cosseddu, P.; Bonfiglio, A. *Thin Solid Films* **2008**, *516*, 1533–1537.
(20) Mamada, M.; Kumaki, D.; Nishida, J.-i.; Tokito, S.; Yamashita, Y. *ACS Appl. Mater. Interfaces* **2010**, *2*, 1303–1307.
(21) Reese, C.; Chung, W. J.; Ling, M. M.; Roberts, M.; Bao, Z. N. *Appl. Phys. Lett.* **2006**, *89*, 202108.
(22) Chabinyc, M. L.; Lu, J. P.; Street, R. A.; Wu, Y. L.; Liu, P.; Ong, B. S. *J. Appl. Phys.* **2004**, *96*, 2063–2070.
(23) Suzuki, K.; Tanaka, T.; Tosaka, Y.; Horie, H.; Arimoto, Y. *IEEE Trans. Electron Devices* **1993**, *40*, 2326–2329.
(24) Qin Jia, C.; Ye, G.; Mary, B. C.-P.; Hong Bin, Y.; Zhi Song, L.; Qun Liang, S.; Chang Ming, L.; Zhi Li, D. *Appl. Phys. Lett.* **2008**, *93*, 113304.
(25) Ong, B. S.; Wu, Y.; Liu, P.; Gardner, S. *J. Am. Chem. Soc.* **2004**, *126*, 3378–3379.
(26) Lawrence, C. *J., Phys. Fluids* **1988**, *31*, 2786–2795.
(27) Rolland, J. P.; Hagberg, E. C.; Denison, G. M.; Carter, K. R.; DeSimone, J. M. *Angew. Chem., Int. Ed.* **2004**, *43*, 5796–5799.
(28) Kuo, A. C. M. In *Polymer Data Handbook*, 2nd ed.; Oxford University Press: New York, 1999.
(29) Gong, G.; Michael, G. K. *Appl. Phys. Lett.* **2008**, *92*, 053305.

(30) Koo, J. B.; Kim, S. H.; Lee, J. H.; Ku, C. H.; Lim, S. C.; Zyung, T. *Synth. Met.* **2006**, *156*, 99–103.
(31) Noh, Y. H.; Young Park, S.; Seo, S.-M.; Lee, H. H. *Org. Electron.* **2006**, *7*, 271–275.
(32) Choi, C. G.; Baez, B. S. *Solid State Lett.* **2007**, *10*, H347–H350.
(33) Lefenfeld, M.; G. B. J., A. R. *Adv. Mater.* **2003**, *15*, 1188–1191.
(34) Takahiko, M.; Hisato, K.; Haruo, K. *Appl. Phys. Lett.* **2006**, *89*, 123508.
(35) Hong, K.; Yang, S. Y.; Yang, C.; Kim, S. H.; Choi, D.; Park, C. E. *Org. Electron.* **2008**, *9*, 864–868.
(36) Cai, Q. J.; Chan-Park, M. B.; Zhang, J.; Gan, Y.; Li, C. M.; Chen, T. P.; Ong, B. S. *Org. Electron.* **2008**, *9*, 14–20.
(37) Nobuhide, Y.; Makoto, N.; Nobukazu, H.; Kazumasa, N.; Masaru, W.; Jiro, K. *Appl. Phys. Lett.* **2004**, *85*, 4663–4665.